

# 2D type-II Dirac fermions in a LaAlO<sub>3</sub>/LaNiO<sub>3</sub>/LaAlO<sub>3</sub> quantum well

L. L. Tao and Evgeny Y. Tsymbal

Department of Physics and Astronomy & Nebraska Center for Materials and Nanoscience  
University of Nebraska, Lincoln, Nebraska 68588, USA

The type-II Dirac fermions that are characterized by a tilted Dirac cone and anisotropic magneto-transport properties have been recently proposed theoretically and confirmed experimentally. Here, we predict the emergence of two-dimensional type-II Dirac fermions in LaAlO<sub>3</sub>/LaNiO<sub>3</sub>/LaAlO<sub>3</sub> quantum-well structures. Using first-principles calculations and model analysis, we show that the Dirac points are formed at the crossing between the  $d_{x^2-y^2}$  and  $d_z^2$  bands protected by the mirror symmetry. The energy position of the Dirac points can be tuned to appear at the Fermi energy by changing the quantum-well width. For the quantum-well structure with a two-unit cell thick LaNiO<sub>3</sub> layer, we predict the coexistence of the type-II Dirac points and the Dirac nodal line. The results are analyzed and interpreted using a tight-binding model and symmetry arguments. Our findings offer a practical way to realize the 2D type-II Dirac fermions in oxide heterostructures.

**Introduction.** The recent proposal of type-II Weyl fermions<sup>1</sup> has inspired intensive investigations of the counterpart type-II Dirac fermions<sup>2,3,4,5</sup>. The type-II Weyl/Dirac fermions merge at the boundary between electron and hole pockets and exhibit specific anisotropic magneto-transport behavior qualitatively different from the type-I Dirac fermions<sup>1,6,7</sup>. To date, a handful of candidates hosting the three-dimensional (3D) type-II Dirac fermions have been theoretically proposed, such as materials deriving from PtSe<sub>2</sub><sup>2</sup>, YPd<sub>2</sub>Sn<sup>3</sup>, VAl<sub>3</sub><sup>4</sup>, and KMnBi<sup>5</sup> families. The experimental evidence of the 3D type-II Dirac fermions in bulk PtSe<sub>2</sub><sup>8,9</sup>, PtTe<sub>2</sub><sup>10</sup>, and PdTe<sub>2</sub><sup>11</sup> have been reported based on angle-resolved photoemission spectroscopy measurements.

The type-II Dirac fermions can also be formed in two-dimensional (2D) systems by analogy to the well-known type-I Dirac fermions in graphene<sup>12</sup> and other 2D systems<sup>13,14,15,16</sup>. For example, the existence of the 2D type-II Dirac fermions have been predicted in monolayer WTe<sub>2</sub><sup>17</sup> and in graphene with nitrogen line defects<sup>18</sup>. However, the properties of these free-standing 2D materials systems are likely to be different when they are deposited on a substrate for performing experimental measurements. For example, the Dirac cone in a free-standing silicene is destroyed due to the hybridization with an Ag(111) substrate<sup>19</sup>. In this regard, it would be desirable to find 2D systems, which can be precisely controlled and not effected by the conditions of measurements. From this point of view, complex oxide heterostructures may serve as a fertile playground to realize the 2D type-II Dirac fermions in practice. Due to advances in thin-film deposition and characterization techniques, the layered oxide heterostructures can be synthesized with atomic-scale precision and exhibit variety of electronic phenomena not found in bulk constituents<sup>20</sup>.

Here, we propose the realization of 2D type-II Dirac fermions in the experimental feasible oxide quantum-well structures LaAlO<sub>3</sub>/LaNiO<sub>3</sub>/LaAlO<sub>3</sub>(001)<sup>21</sup>. Bulk LaNiO<sub>3</sub> (LNO) is a paramagnetic metal<sup>22</sup>, which can be used as an oxide

electrode<sup>23,24</sup>, while bulk LaAlO<sub>3</sub> (LAO) is a wide-gap insulator<sup>25</sup>. Previous work on LNO/LAO (001) heterostructures was focused on the orbital engineering to produce novel electronic properties<sup>26-29</sup>. Here, we exploit the effect of quantum confinement of the LNO layer to form the emerging electronic states. We predict that the type-II Dirac points (DPs) appear along the diagonal axes of the 2D Brillouin zone (BZ) and the band dispersion around the DP is strongly anisotropic in the momentum space. The energy position of the Dirac points can be tuned by changing the quantum-well width. Given the experimentally feasible structure with tunable degrees of freedom, the proposed LAO/LNO/LAO quantum-well system represents a promising candidate to realize the 2D type-II Dirac fermions in practice.

**Results and discussion.** First, we investigate the atomic and electronic structure of a monolayer-thick LAO/(LNO)<sub>1</sub>/(LAO) quantum well depicted in Fig. 1(a). Fig. 1(b) shows the calculated relative metal-oxygen (M-O) displacements across the heterostructure. Overall, we see that the displacements are quite small with the slight enhancement  $\sim 0.03$  Å at the interfaces. This stems from no electrostatic mismatch across the interface, due to the equal formal valence of the (NiO<sub>2</sub>)<sup>-</sup> and (AlO<sub>2</sub>)<sup>-</sup> atomic layers. This is contrast to the well-known SrTiO<sub>3</sub>/LaAlO<sub>3</sub> (001) system where a large La-O displacement at the interface  $\sim 0.2$  Å is produced due to the electrostatic mismatch between the charged (LaO)<sup>+</sup> and neutral (TiO<sub>2</sub>)<sup>0</sup> atomic layers<sup>30</sup>. Fig. 1(c) shows the local density of states (LDOS) across the quantum well. It is seen that the LDOS at the Fermi energy  $E_F$  is non-zero only within the LNO unit cell (u.c.), suggesting a nearly perfect 2D electron gas. Examining the LDOS of the LNO layer suggests that the Ni- $t_{2g}$  ( $d_{xy}, d_{yz}, d_{zx}$ ) orbitals are well below  $E_F$  and fully occupied, whereas the Ni- $e_g$  ( $d_{x^2-y^2}, d_z^2$ ) orbitals are partially occupied and thus determine the electronic structure around the Fermi energy.

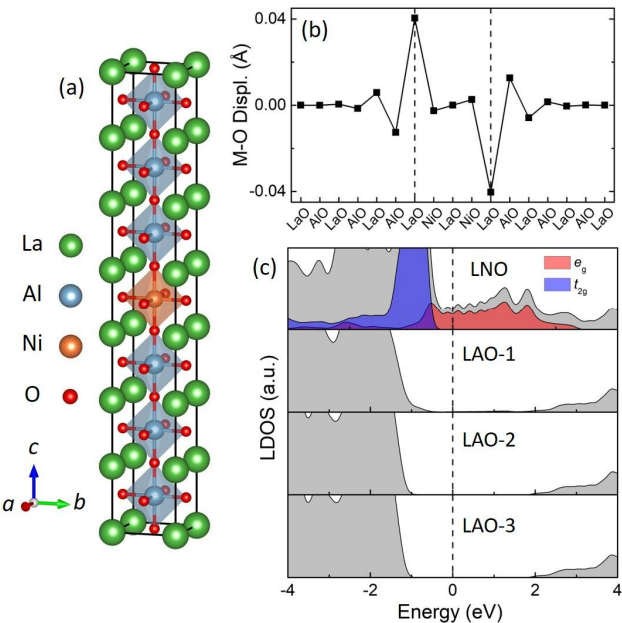


FIG. 1. (a) Atomic structure of the LAO/(LNO)<sub>1</sub>/LAO (001) quantum well. Here  $(a, b, c)$  axes is concordant with the  $(x, y, z)$  axes. (b) The relative metal-O (M-O) displacements. The two vertical dashed lines denote interfaces. (c) Local density of states (LDOS) on layers from LNO (top) to deep LAO-3 (bottom). The vertical dashed line denotes the Fermi energy.

Next, we discuss the electronic structure of the LAO/(LNO)<sub>1</sub>/LAO quantum well. Fig. 2(a) shows the calculated band structure without spin-orbit coupling (SOC). It is seen that the  $d_{x^2-y^2}$  and  $d_{z^2}$  bands cross each other along the  $\Gamma$ -M direction. Zooming in around the crossing point ( $\sim 0.8$  eV above  $E_F$ ) reveals a linear dispersion, which is strongly anisotropic in  $k$  space [Figs. 2(b) and 2(c)]. The band crossing is tilted along the  $\Gamma$ -M line [Fig. 2(b)], while it is straight perpendicular to the  $\Gamma$ -M line [Fig. 2(c)]. Fig. 2(d) shows the 3D band structure around the crossing point. It is seen that cutting the bands by the isoenergy plane opens electron and hole pockets touching at the crossing point. Due to space inversion symmetry  $P$  and time-reversal symmetry  $T$ , each band in the quantum-well structure represents a Kramers doublet which makes the crossing point fourfold degenerate. These properties are the characteristic features of the type-II Dirac fermion and the crossing point is the well-known DP. Due to the  $C_4$  four-fold rotation symmetry, there are four equivalent DPs in the 2D BZ [red dots in the inset of Fig. 1(a)].

The DPs are protected by the mirror symmetry. Along the  $\Gamma$ -M line, wave vector  $\mathbf{k}$  is invariant under the symmetry operations  $M_{xy}$  of the diagonal mirror plane, which lies perpendicular to the  $k_y = -k_x$  axis. In the spinless case (i.e. in absence of SOC),  $M_{xy}^2 = 1$  and hence all the bands at the  $\Gamma$ -M

line can be denoted by the eigenvalues ( $\pm 1$ ) of  $M_{xy}$ . It is evident that  $M_{xy} |x^2 - y^2\rangle = - |x^2 - y^2\rangle$  and  $M_{xy} |z^2\rangle = |z^2\rangle$  (here  $|\mathbf{L}\rangle$  denotes the orbital basis). The different eigenvalues (and hence different irreducible representations) forbid the hybridization between the  $d_{x^2-y^2}$  and  $d_{z^2}$  bands. The DP is therefore protected by the  $M_{xy}$  symmetry and cannot be gapped.

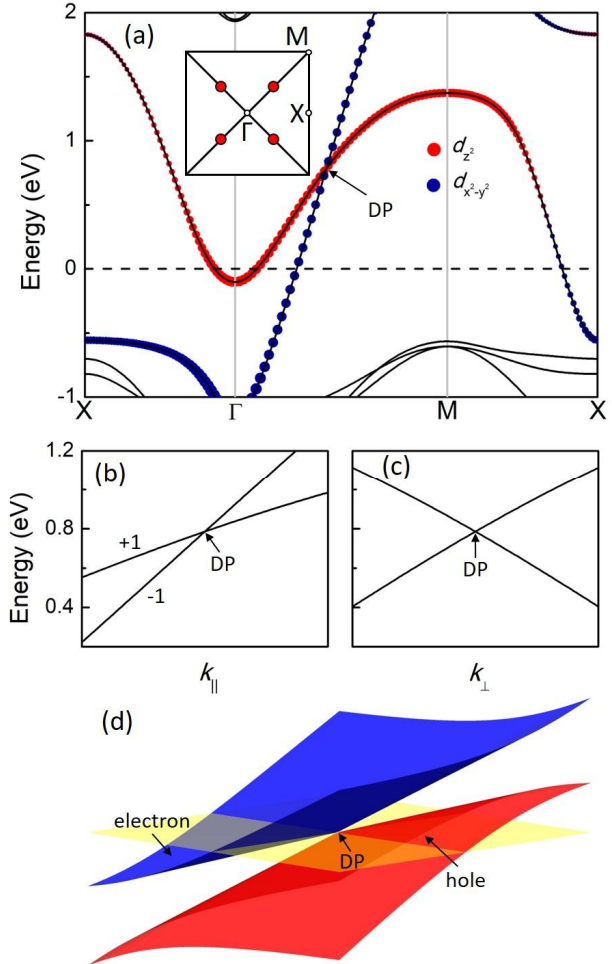


FIG. 2. (a) Band structure of the LAO/(LNO)<sub>1</sub>/LAO (001) quantum well along the high symmetry lines  $X(\pi, 0) - \Gamma(0, 0) - M(\pi, \pi) - X(\pi, 0)$  without SOC. Projection onto the  $e_g$  ( $d_{x^2-y^2}$ ,  $d_{z^2}$ ) orbitals is indicated by dots which size corresponds to the weight of each orbital. Inset: the 2D BZ. Positions of DPs are indicated by the red dots. Zoom-in band structure around the DP (b) along the  $\Gamma$ -M direction ( $k_p$ ) and (c) perpendicular to the  $\Gamma$ -M direction ( $k_\perp$ ). (d) 3D band structure around the DP. The light yellow plane represents the isoenergy cutting through the DP with electron and hole pockets indicated.

To gain further insight into the nature of the DPs, we derive the  $\mathbf{k} \times \mathbf{p}$  effective Hamiltonian based on symmetry analysis<sup>31</sup>.

The Hamiltonian up to the linear order in  $k$  around the DP  $\mathbf{k}_0$  is expressed as follows

$$H(\mathbf{k}_0 + \mathbf{q}) = E(\mathbf{k}_0) + \sum_{i,j} d_{ij} \mathbf{s}_i q_j, \quad (1)$$

where  $\mathbf{s}_i$  are the  $2 \times 2$  unitary matrix ( $i = 0$ ) or the Pauli matrices ( $i = x, y, z$ ) acting within the  $(|x^2 - y^2\rangle, |z^2\rangle)$  orbital space,  $\mathbf{q}$  is the wave vector deviation from  $\mathbf{k}_0$  and  $q_j$  ( $j = x, y, z$ ) are its projections, and  $d_{ij}$  are the expansion coefficients. The symmetry operations at the DP are  $PT$  and  $M_{xy}$ . Since  $PT = \mathbf{s}_0 K$  ( $K$  represents the complex conjugation) and  $M_{xy} = -\mathbf{s}_z$  in the spinless case, collecting all the symmetry allowed  $k$ -dependent terms reduces Eq. (1) to

$$H = d_0 (q_x + q_y) + d_z \mathbf{s}_z (q_x + q_y) + d_x \mathbf{s}_x (q_x - q_y). \quad (2)$$

The energy spectrum of Eq. (2) is

$$E_{\pm} = d_0 (q_x + q_y) \pm \sqrt{d_z^2 (q_x + q_y)^2 + d_x^2 (q_x - q_y)^2}. \quad (3)$$

Eq. (3) describes the 2D anisotropic Dirac fermions. Fitting to the band dispersion around the DP yields  $d_0 = 2.33$  eV Å,  $d_z = 1.03$  eV Å, and  $d_x = 2.13$  eV Å. Along the  $\Gamma$ -M line,  $q_x = q_y$  and the Dirac cone is strongly tilted due to  $d_0 > d_z$ .

We see that the LAO/(LNO)<sub>2</sub>/LAO quantum-well structure hosts the 2D type-II Dirac fermions due to the symmetry protected band crossing between the two  $e_g$  bands. However, the energy position of the DP is relatively high, i.e.  $\sim 0.8$  eV above  $E_F$ . Electron doping or gate biasing are technically feasible to tune the DP closer to  $E_F$ . However, there is another efficient way to tune the DP by changing the quantum-well width (LNO layer thickness).

Fig. 3(a) shows the calculated band structure of the LAO/(LNO)<sub>2</sub>/LAO (001) quantum well. Comparison to Fig. 2(a) reveals that the quantum confinement in the  $z$  direction splits the two  $d_z^2$  bands: at the  $\Gamma$  point, one band shifts above  $E_F$  while the other band moves below  $E_F$ . On the other hand, the dispersion of the  $d_{x^2-y^2}$  bands is nearly unaffected (due to the  $d_{x^2-y^2}$  orbitals lying in the  $xy$ -plane). As a result, the two crossing points between the lower  $d_z^2$  band and the two  $d_{x^2-y^2}$  bands become closer to  $E_F$ . These crossing points, denoted by DP1 and DP2, are seen in Fig. 3(b) along the  $\Gamma$ -M line ( $k_p$ ). Figs. 3(c) and 3(d) show the band dispersions along the lines perpendicular to  $\Gamma$ -M ( $k_{\perp}$ ) and passing through the DP1 and DP2 points, respectively. It is seen that DP1 exhibits properties

similar to the DP in the LAO/(LNO)<sub>1</sub>/LAO quantum well: the linear dispersion in all directions, the tilted band crossing along the  $\Gamma$ -M line [Fig. 3(b)], and the straight band crossing perpendicular to the  $\Gamma$ -M line [Fig. 3(c)]. DP2 reveals however a different behavior: along the  $\Gamma$ -M line, the crossing bands have the tilted linear dispersion [Fig. 3(b)], while along the line perpendicular to  $\Gamma$ -M, the dispersion is quadratic [Fig. 3(d)]. Using a tight-binding (TB) model (discussed below), we have calculated the 3D band dispersion around  $E_F$ . Fig. 4(a) shows that DP1 emerges as an isolated point, while DP2 belongs to a closed Dirac nodal line (DNL). It is evident from Fig. 4(b) that the energy of the DNL varies from  $-0.04$  eV to  $-0.7$  eV, which favors the experimental measurement over a large energy scale.

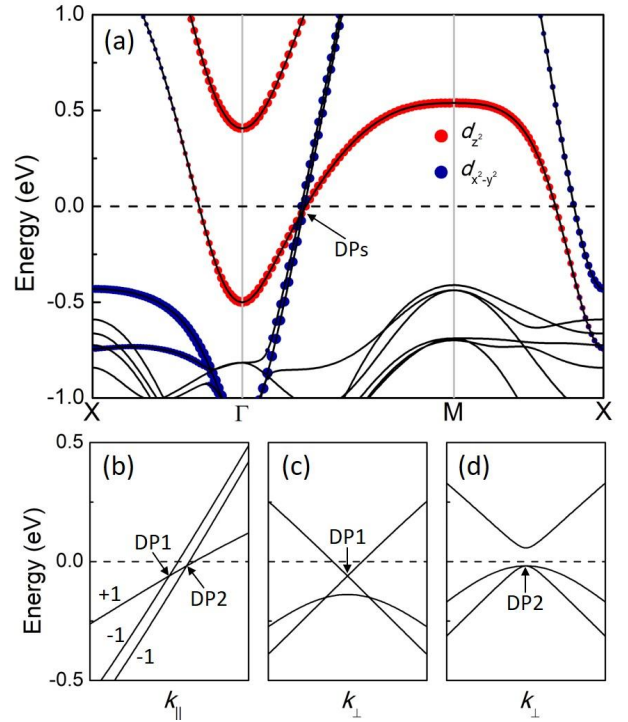


FIG. 3. (a) Band structure of the LAO/(LNO)<sub>2</sub>/LAO (001) quantum well without SOC. Projection onto the  $e_g$  ( $d_{x^2-y^2}$ ,  $d_z^2$ ) orbitals is indicated by dots which size corresponds to the weight of each orbital. (b, c, d) Zoom-in band structures around the DPs. (b) The band dispersion is along the  $\Gamma$ -M direction ( $k_p$ ) and (c, d) perpendicular to the  $\Gamma$ -M directions ( $k_{\perp}$ ) and passing through DP1 (c) and DP2 (d).

The DNL appears due to the  $PT$  symmetry, which in general produces a closed nodal loop in the BZ<sup>32,33,34</sup>. The point group for a general crossing point at the DNL is  $C_s$ , which consists of the identity element  $E$  and the mirror reflection  $M_z$  with respect to the plane perpendicular to the  $z$  axis. There are two irreducible representations of the  $C_s$  group<sup>35</sup>,  $A_{\text{1g}}$  and  $A_{\text{2g}}$ . Examining the two bands crossing the DP at the DNL [Fig. S4a in Supporting Information (SI)], we find that one band belongs

to the  $A\bar{A}$  representation, while the other band belongs to the  $A\bar{C}$  representation. Since the eigenvalue of  $M_z$  for the  $A\bar{A}A\bar{C}$  representation is  $+1$  ( $-1$ )<sup>35,36</sup>, the DNL is protected by the mirror symmetry  $M_z$ .

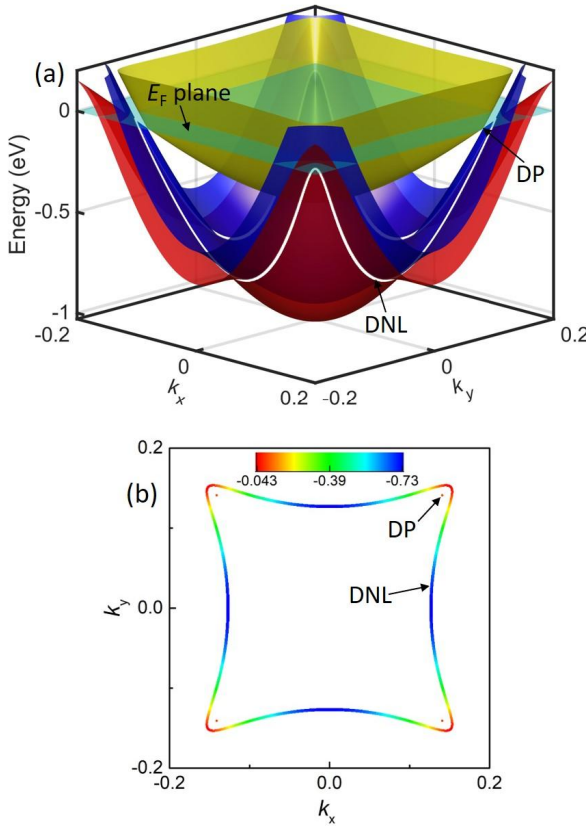


FIG. 4. (a) 3D band structure around the Fermi energy. Band touching points between red and blue branches form the Dirac nodal line (DNL) (white loop). (b) 2D projection of the isolated Dirac points (DP) and the closed DNL.  $k_x$  and  $k_y$  are in units of  $2\pi/a$ . The color map quantifies the band energies at the touching points. The results are obtained using the tight-binding Hamiltonian model as described in text.

To obtain a deeper microscopic insight into the band structure of the LAO/LNO/LAO quantum wells, we construct a TB Hamiltonian of the system in basis of the  $|x^2 - y^2\rangle$  and  $|z^2\rangle$  orbitals. Denoting these orbitals as  $|a\rangle$  and  $|b\rangle$ , Hamiltonian  $H_1$  for LAO/(LNO)<sub>1</sub>/LAO reads (SI, sec.1)

$$H_1 = \frac{1}{2}(h_a + h_b)\mathbf{s}_0 + \frac{1}{2}(h_a - h_b)\mathbf{s}_z + h_{ab}\mathbf{s}_x, \quad (4)$$

where  $\mathbf{s}_0$  is the  $2 \times 2$  unitary matrix and  $\mathbf{s}_{x,z}$  are the Pauli matrices acting in the  $(|a\rangle, |b\rangle)$  orbital space. The hopping

parameters  $h$  are functions of  $(k_x, k_y)$  and are given in SI. The energy spectrum of Eq. (4) is

$$\mathbf{e}_\pm = \frac{1}{2}(h_a + h_b) \pm \frac{1}{2}\sqrt{(h_a - h_b)^2 + 4h_{ab}^2}. \quad (5)$$

Hamiltonian  $H_2$  for LAO/(LNO)<sub>2</sub>/LAO can be constructed from  $H_1$ . To describe an additional degree of freedom resulting from the presence of two LNO layers, we introduce another set of the Pauli matrices  $\tau$ .  $H_2$  reads (SI, sec.1)

$$H_2 = t_0 \tilde{\mathbf{A}} H_1 + t_x \tilde{\mathbf{A}} H_z, \quad (6)$$

where  $H_z = \frac{1}{2}(h_{az} + h_{bz})\mathbf{s}_0 + (h_{az} - h_{bz})\mathbf{s}_z + 2h_{abz}\mathbf{s}_x$  and the hopping parameters  $h$  are given in SI. The energy spectrum of Eq. (6) is

$$\begin{aligned} \mathbf{e}_{1,2} &= \frac{1}{2}(h_a + h_b - h_{az} - h_{bz}) \\ &\pm \frac{1}{2}\sqrt{(h_a - h_b - h_{az} + h_{bz})^2 + 4(h_{ab} - h_{abz})^2} \\ \mathbf{e}_{3,4} &= \frac{1}{2}(h_a + h_b + h_{az} + h_{bz}) \\ &\pm \frac{1}{2}\sqrt{(h_a - h_b + h_{az} - h_{bz})^2 + 4(h_{ab} + h_{abz})^2} \end{aligned} \quad (7)$$

Along the  $\Gamma$ -M ( $k_x = k_y$ ) direction,  $h_{ab} = h_{abz} = 0$  and Eqs. (5) and (7) are reduced to  $\mathbf{e}_\pm = h_b, h_a$  and  $\mathbf{e}_{1,4} = h_b \mp h_{bz}$ ,  $\mathbf{e}_{2,3} = h_a \mp h_{az}$ , respectively.  $h_a$  ( $d_{x^2-y^2}$ ) and  $h_b$  ( $d_z^2$ ) are the two band energies along the  $\Gamma$ -M line for LAO/(LNO)<sub>1</sub>/LAO. In case of LAO/(LNO)<sub>2</sub>/LAO, both  $h_a$  and  $h_b$  are split into two subbands with the splitting energy being proportional to  $2h_{az}$  and  $2h_{bz}$ , respectively. Since the  $|a\rangle$  ( $|b\rangle$ ) orbital lies in (out of) the plane, the hopping  $h_{az}$  is expected to be much smaller than  $h_{bz}$ , which is confirmed by the fitting (SI, Table S1). Consequently, the splitting between the two  $d_z^2$  bands is significantly larger than the splitting between the two  $d_{x^2-y^2}$  bands, which is in line with our DFT results [Fig. 3(a)]. The fitted parameters and the explicit comparison between the DFT and TB results can be found in SI.

It is noteworthy that the previous experimental work<sup>37,38</sup> has demonstrated a metal-insulator transition (MIT) in a few-unit-cell-thick LNO film due to the low dimensionality and strain. However, very recently it was demonstrated that oxygen vacancies play a critical role in triggering a MIT<sup>39</sup>. Moreover, both the DFT and DFT+DMFT (dynamical mean field theory)

results reveal the metallic feature even for one u.c. LNO film without oxygen vacancies<sup>39</sup>, in agreement with our results.

Finally, we discuss the effect of SOC on the DPs from symmetry arguments. Here we consider a LAO/(LNO)<sub>1</sub>/LAO quantum well as an example, but the same conclusion applies to LAO/(LNO)<sub>2</sub>/LAO as well. Along the  $\Gamma$ -M line, there are two symmetry invariant operations, i.e.  $PT$  and  $M_{xy}$ . In real space, it can be easily checked that  $\langle \hat{e}PT, M_{xy} \rangle = 0$ . In spin space, we have  $PT = i\mathbf{S}_y K$  and  $M_{xy} = \frac{i}{\sqrt{2}}(\mathbf{S}_x - \mathbf{S}_y)$ . Combining real and spin space, we obtain  $\langle \hat{e}PT, M_{xy} \rangle = 0$  and  $M_{xy}^2 = -1$ . Since along the  $\Gamma$ -M line,  $\langle \hat{e}M_{xy}, H_1 \rangle = 0$ , the Bloch states  $|\psi\rangle$  and  $PT|\psi\rangle$  can be labeled using the eigenvalues of  $M_{xy}$ , namely  $M_{xy}|\psi\rangle = \pm i|\psi\rangle$  and  $M_{xy}PT|\psi\rangle = \mp iPT|\psi\rangle$ . The doubly degenerate states  $|\psi\rangle$  and  $PT|\psi\rangle$  have opposite  $M_{xy}$  eigenvalues. Therefore, when two sets of such doublet bands cross at the DP, the two bands with the same  $M_{xy}$  eigenvalue can hybridize and open a gap at the DP, as schematically shown in Figs. S3(b) and S3(c). To confirm this, we have calculated the band structure by including SOC. As shown in the Fig. S4, a tiny gap of  $\sim 2$  meV appears at the DP. Thus, in the spinful case, the DP is not protected, and a small gap opens due to SOC. The same conclusion applies to the DNL (Fig. S5).

**Summary.** In summary, we have predicted that LAO/LNO/LAO (001) quantum-well structures host the 2D type-II Dirac fermions. Our DFT calculations and TB modeling demonstrate that a unit-cell-thick LNO layer, when placed in the quantum well, forms the Dirac points that are located along the diagonal lines of the 2D Brillouin zone and in the spinless case are protected by the mirror symmetry. The formation of the 2D type-II Dirac fermions can be tuned by the quantum-well

width. For a two-unit-cell LNO layer, the energy position of the Dirac point is found to appear near the Fermi energy. In this case, we predict the coexistence of the isolated Dirac points and a closed Dirac nodal line. Spin-orbit coupling opens a small ( $\sim 2$  meV) gap at the Dirac points and the Dirac nodal line. We hope that our findings will stimulate the experimental search for the 2D type-II Dirac fermions in the LAO/LNO/LAO (001) quantum-well structures.

**Computational methods.** Density-functional theory (DFT) calculations are performed using the plane-wave ultrasoft pseudopotential method<sup>40</sup> implemented in Quantum-ESPRESSO<sup>41</sup>. An energy cutoff of 680 eV and local density approximation (LDA)<sup>42</sup> for the exchange and correlation functional are used throughout. The LAO/LNO/LAO quantum-well structure is modelled using (LNO)<sub>n</sub>/(LAO)<sub>6</sub> ( $n = 1, 2$ ) superlattices, as shown in Fig. 1(a) for  $n=1$ . The in-plane lattice constant  $a$  of the superlattices is fixed to the calculated lattice constant of bulk cubic LAO,  $a=3.757$  Å, to simulate epitaxial growth on a LAO substrate. The out-of-plane lattice constant as well as the atomic positions are fully relaxed with the force tolerance of 2.6 meV/Å. Previous work<sup>43</sup> shows that the conventional LDA method gives the best agreement with the experimental data for LNO. As a comparison, the Hubbard  $U$  correction for Ni- $d$  electron is included<sup>44</sup> to consider the correlation effects, as presented in section 3 of SI.

**Author contributions.** L.L.T. and E.Y.T conceived the project. L.L.T. carried out the calculations. Both authors discussed the results and wrote the manuscript.

**Acknowledgments.** This work was supported by the National Science Foundation (NSF) through Nebraska Materials Research Science and Engineering Center (MRSEC) (NSF Grant No. DMR-1420645). Computations were performed at the University of Nebraska Holland Computing Center. The atomic structure was produced using VESTA software<sup>45</sup>.

<sup>1</sup> Soluyanov, A. A.; Gresch, D.; Wang, Z.; Wu, Q.; Troyer, M.; Dai, X.; Bernevig, B. A. Type-II Weyl semimetals. *Nature* 2015, 527, 495–498.

<sup>2</sup> Huang, H.; Zhou, S.; Duan, W. Type-II Dirac fermions in the PtSe<sub>2</sub> class of transition metal dichalcogenides. *Phys. Rev. B: Condens. Matter Mater. Phys.* 2016, 94, 121117(R).

<sup>3</sup> Guo, P. J.; Yang, H. C.; Liu, K.; Lu, Z. Y. Type-II Dirac semimetals in the YPd<sub>2</sub>Sn class. *Phys. Rev. B: Condens. Matter Mater. Phys.* 2017, 95, 155112.

<sup>4</sup> Chang, T. R.; Xu, S. Y.; Sanchez, D. S.; Tsai, W. F.; Huang, S. M.; Chang, G.; Hsu, C. H.; Bian, G.; Belopolski, I.; Yu, Z. M.; Yang, S. A.; Neupert, T.; Jeng, H. T.; Lin, H.; Hasan, M. Z. Type-II Symmetry-Protected Topological Dirac Semimetals. *Phys. Rev. Lett.* 2017, 119, 026404.

<sup>5</sup> Le, C.; Qin, S.; Wu, X.; Dai, X.; Fu, P.; Fang, C.; Hu, J. Three-dimensional topological critical Dirac semimetal in AMgBi (A=K, Rb, Cs). *Phys. Rev. B: Condens. Matter Mater. Phys.* 2017, 96, 115121.

<sup>6</sup> Yu, Z. M.; Yao, Y.; Yang, S. A. Predicted Unusual Magnetoresponse in Type-II Weyl Semimetals. *Phys. Rev. Lett.* 2016, 117, 077202.

<sup>7</sup> Tchoumakov, S.; Civelli, M.; Goerbig, M. O. Magnetic-Field Induced Relativistic Properties in Type-I and Type-II Weyl Semimetals. *Phys. Rev. Lett.* 2016, 117, 086402.

<sup>8</sup> Zhang, K.; Yan, M.; Zhang, H.; Huang, H.; Arita, M.; Sun, Z.; Duan, W.; Wu, Y.; Zhou, S. Experimental evidence for type-II Dirac semimetal in PtSe<sub>2</sub>. *Phys. Rev. B: Condens. Matter Mater. Phys.* 2017, 96, 125102.

<sup>9</sup> Li, Y.; Xia, Y.; Ekahana, S. A.; Kumar, N.; Jiang, J.; Yang, L.; Chen, C.; Liu, C.; Yan, B.; Felser, C.; Li, G.; Liu, Z.; Chen, Y. Topological origin of the type-II Dirac fermions in PtSe<sub>2</sub>. *Phys. Rev. Materials* 2017, 1, 074202.

<sup>10</sup> Yan, M.; Huang, H.; Zhang, K.; Wang, E.; Yao, W.; Deng, K.; Wan, G.; Zhang, H.; Arita, M.; Yang, H. Lorentz-violating type-II Dirac fermions in transition metal dichalcogenide PtTe<sub>2</sub>. *Nat. Commun.* 2017, 8, 257.

<sup>11</sup> Noh, H. J.; Jeong, J.; Cho, E. J.; Kim, K.; Min, B. I.; Park, B. G. Experimental Realization of Type-II Dirac Fermions in a PdTe<sub>2</sub> Superconductor. *Phys. Rev. Lett.* 2017, 119, 016401.

<sup>12</sup> Castro Neto, A. H.; Guinea, F.; Peres, N. M. R.; Novoselov, K. S.; Geim, A. K. The electronic properties of graphene. *Rev. Mod. Phys.* 2009, 81, 109-162.

<sup>13</sup> Park C. H.; Louie S. G. Making Massless Dirac Fermions from a Patterned Two-Dimensional Electron Gas. *Nano Lett.* 2009, 9, 1793-1797.

<sup>14</sup> Tianyi Cai, T.; Li, X.; Wang, F.; Ju, S.; Feng, J.; Gong, C. D. Single-Spin Dirac Fermion and Chern Insulator Based on Simple Oxides. *Nano Lett.* 2015, 15, 6434-6439.

<sup>15</sup> Baik S. S.; Kim, K. S.; Yi, Y.; Choi H. J. Emergence of Two-Dimensional Massless Dirac Fermions, Chiral Pseudospins, and Berry's Phase in Potassium Doped Few-Layer Black Phosphorus. *Nano Lett.* 2015, 15, 7788-7793.

<sup>16</sup> Zhang, H.; Li, Y.; Hou, J.; Du, A.; Chen, Z. Dirac State in the FeB<sub>2</sub> Monolayer with Graphene-Like Boron Sheet. *Nano Lett.* 2016, 16, 6124-6129.

<sup>17</sup> Muechler, L.; Alexandradinata, A.; Neupert, T.; Car, R. Topological Nonsymmorphic Metals from Band Inversion. *Phys. Rev. X* 2016, 6, 041069.

<sup>18</sup> Zhang, H.; Xie, Y.; Zhong, C.; Zhang, Z.; Chen, Y. Tunable Type-I and Type-II Dirac Fermions in Graphene with Nitrogen Line Defects. *J. Phys. Chem. C* 2017, 121, 12476-12482.

<sup>19</sup> Wang, Y. P.; Cheng, H. P. Absence of a Dirac cone in silicene on Ag(111): First-principles density functional calculations with a modified effective band structure technique. *Phys. Rev. B: Condens. Matter Mater. Phys.* 2013, 87, 245430.

<sup>20</sup> Hwang, H. Y.; Iwasa, Y.; Kawasaki, M.; Keimer, B.; Nagaosa N.; Tokura, Y. Emergent phenomena at oxide interfaces. *Nature Mater.* 2012, 11, 103-113.

<sup>21</sup> Wrobel, F.; Mark, A. F.; Christiani, G.; Sigle, W.; Habermeier, H. U.; van Aken, P. A.; Logvenov, G.; Keimer, B.; Benckiser, E. Comparative study of LaNiO<sub>3</sub>/LaAlO<sub>3</sub> heterostructures grown by pulsed laser deposition and oxide molecular beam epitaxy. *Appl. Phys. Lett.* 2017, 110, 041606.

<sup>22</sup> Medarde, M. L. Structural, magnetic and electronic properties of RNiO<sub>3</sub> perovskites (R=rare earth). *J. Phys.: Condens. Matter* 1997, 9, 1679.

<sup>23</sup> Peng, J. J.; Song, C.; Cui, B.; Li, F.; Mao, H. J.; Wang, G. Y.; Pan, F. Manipulation of orbital occupancy by ferroelectric polarization in LaNiO<sub>3</sub>/BaTiO<sub>3-δ</sub> heterostructures. *Appl. Phys. Lett.* 2015, 107, 182904.

<sup>24</sup> Tao, L. L.; Wang, J. Ferroelectricity and tunneling electroresistance effect driven by asymmetric polar interfaces in all-oxide ferroelectric tunnel junctions. *Appl. Phys. Lett.* 2016, 108, 062903.

<sup>25</sup> Bjaalie1, L.; Himmetoglu, B.; Weston, L.; Janotti A.; Van de Walle, C. G. Oxide interfaces for novel electronic applications. *New J. Phys.* 2014, 16, 025005.

<sup>26</sup> Hansmann, P.; Yang, X.; Toschi, A.; Khaliullin, G.; Andersen, O. K.; Held, K. Turning a Nickelate Fermi Surface into a Cupratelike One through Heterostructuring. *Phys. Rev. Lett.* 2009, 103, 016401.

<sup>27</sup> Han, M. J.; Marianetti, C. A.; Millis, A. J. Chemical control of orbital polarization in artificially structured transition-metal oxides: La<sub>2</sub>NiXO<sub>6</sub> (X=B, Al, Ga, In) from first principles. *Phys. Rev. B: Condens. Matter Mater. Phys.* 2010, 82, 134408.

<sup>28</sup> Benckiser, E.; Haverkort, M. W.; Brück, S.; Goering, E.; Macke, S.; Frañó, A.; Yang, X.; Andersen, O. K.; Cristiani, G.; Habermeier, H. U.; Boris, A. V.; Zegkinoglou, I.; Wochner, P.; Kim, H. J.; Hinkov, V.; Keimer, B. Orbital reflectometry of oxide heterostructures. *Nature Mater.* 2011, 10, 189-193.

<sup>29</sup> Disa, A. S.; Kumah, D. P.; Malashevich, A.; Chen, H.; Arena, D. A.; Specht, E. D.; Ismail-Beigi, S.; Walker, F. J.; Ahn, C. H. Orbital Engineering in Symmetry-Breaking Polar Heterostructures. *Phys. Rev. Lett.* 2015, 114, 026801.

<sup>30</sup> Pentcheva, R.; Arras, R.; Otte, K.; Ruiz, V. G.; Pickett, W. E. Termination control of electronic phases in oxide thin films and interfaces: LaAlO<sub>3</sub>/SrTiO<sub>3</sub>(001). *Phil. Trans. R. Soc. A* 2012, 370, 4904-4926.

<sup>31</sup> Tao, L. L.; Paudel, T. R.; Kovalev, A. A.; Tsymbal, E. Y. Reversible spin texture in ferroelectric HfO<sub>2</sub>. *Phys. Rev. B: Condens. Matter Mater. Phys.* 2017, 95, 245141.

<sup>32</sup> Herring, C. Accidental Degeneracy in the Energy Bands of Crystals. *Phys. Rev.* 1937, 52, 365.

<sup>33</sup> Quan, Y.; Yin, Z. P.; Pickett, W. E. Single Nodal Loop of Accidental Degeneracies in Minimal Symmetry: Triclinic CaAs<sub>3</sub>. *Phys. Rev. Lett.* 2017, 118, 176402.

<sup>34</sup> Weng, H.; Liang, Y.; Xu, Q.; Yu, R.; Fang, Z.; Dai, X.; Kawazoe, Y. Topological node-line semimetal in three-dimensional graphene networks. *Phys. Rev. B: Condens. Matter Mater. Phys.* 2015, 92, 045108.

<sup>35</sup> Bradley C. J.; Cracknell, A. P. *The mathematical theory of symmetry in solids: representation theory for point groups and space groups* (Oxford: Clarendon Press, 1972).

<sup>36</sup> The orbital functions for the A $\phi$  and A $\phi$  representations are as follows:  $|A\phi\rangle = c_1(|x^2 - y^2\rangle_A + |x^2 - y^2\rangle_B) + c_2(|z^2\rangle_A + |z^2\rangle_B)$  and  $|A\phi\rangle = c_3(|x^2 - y^2\rangle_A - |x^2 - y^2\rangle_B) + c_4(|z^2\rangle_A - |z^2\rangle_B)$ , where the subscripts A and B represent the two Ni sites and  $c_i$  ( $i = 1 - 4$ ) are expansion coefficients. Since  $M_z$  exchanges A and B sites while leaves  $|x^2 - y^2\rangle$  and  $|z^2\rangle$  invariant, it is easy to see that  $M_z|A\phi\rangle = +|A\phi\rangle$  and  $M_z|A\phi\rangle = -|A\phi\rangle$ . These results are confirmed by our DFT calculations.

<sup>37</sup> Boris, A. V.; Matiks, Y.; Benckiser, E.; Frano, A.; Popovich, P.; Hinkov, V.; Wochner, P.; Castro-Colin, M.; Detemple, E.; Malik, V. K.; Bernhard, C.; Prokscha, T.; Suter, A.; Salman, Z.; Morenzoni, E.; Cristiani, G.; Habermeier, H. U.; Keimer, B. Dimensionality Control of Electronic Phase Transitions in Nickel-Oxide Superlattices. *Science* 2011, 332, 937-940.

<sup>38</sup> Scherwitzl, R.; Gariglio, S.; Gabay, M.; Zubko, P.; Gibert, M.; Triscone, J. M. Metal-Insulator Transition in Ultrathin LaNiO<sub>3</sub> Films. *Phys. Rev. Lett.* 2011, 106, 246403.

<sup>39</sup> Golalikhani, M.; Lei, Q.; Chandrasena, R. U.; Kasaei, L.; Park, H.; Bai, J.; Orgiani, P.; Ciston, J.; Sterbinsky, G. E.; Arena, D. A.; Shafer, P.; Arenholz, E.; Davidson, B. A.; Millis, A. J.; Gray, A. X.; Xi, X. X. Nature of the metal-insulator transition in few-unit-cell-thick LaNiO<sub>3</sub> films. *Nat. Commun.* 2018, 9, 2206.

<sup>40</sup> Vanderbilt, D. Soft self-consistent pseudopotentials in a generalized eigenvalue formalism. *Phys. Rev. B: Condens. Matter Mater. Phys.* 1990, 41, 7892(R).

<sup>41</sup> Giannozzi, P.; Baroni, S.; Bonini, N.; Calandra, M.; Car, R.; Cavazzoni, C.; Ceresoli, D.; Chiarotti, G. L.; Cococcioni, M.; Dabo, I. *et al.* QUANTUM ESPRESSO: a modular and open-source software project for quantum simulations of materials. *J. Phys.: Condens. Matter* 2009, 21, 395502.

<sup>42</sup> Perdew, J. P.; Zunger, A. Self-interaction correction to density-functional approximations for many-electron systems. *Phys. Rev. B: Condens. Matter Mater. Phys.* 1981, 23, 5048.

<sup>43</sup> Gou, G.; Grinberg, I.; Rappe, A. M.; Rondinelli, J. M. Lattice normal modes and electronic properties of the correlated metal LaNiO<sub>3</sub>. *Phys. Rev. B: Condens. Matter Mater. Phys.* 2011, 84, 144101.

<sup>44</sup> Cococcioni, M.; de Gironcoli, S. Linear response approach to the calculation of the effective interaction parameters in the LDA+U method. *Phys. Rev. B: Condens. Matter Mater. Phys.* 2005, 71, 035105.

<sup>45</sup> Momma K.; Izumi, F. VESTA 3 for three-dimensional visualization of crystal, volumetric and morphology data. *J. Appl. Cryst.* 2011, 44, 1272-1276.